Published in final edited form as:
Biochemistry. 2012 July 3; 51(26): 5276–5284. doi:10.1021/bi300382d.

Biophysical Investigation of the Ironome of Human Jurkat Cells and Mitochondria

Nema D. Jhurry[1], **Mrinmoy Chakrabarti**[2], **Sean P. McCormick**[2], **Gregory P. Holmes-Hampton**[2], and **Paul A. Lindahl**[1,2,*]

[1]Department of Biochemistry and Biophysics, Texas A&M University, College Station, TX 77843-2128

[2]Department of Chemistry, Texas A&M University, College Station, TX 77843-3255

Abstract

The speciation of iron in intact human Jurkat leukemic cells and their isolated mitochondria was assessed using biophysical methods. Large-scale cultures were grown in medium enriched with ^{57}Fe citrate. Mitochondria were isolated anaerobically to prevent oxidation of iron centers. 5 K Mössbauer spectra of cells were dominated by a sextet due to ferritin. They also exhibited an intense central quadrupole doublet due to S = 0 $[Fe_4S_4]^{2+}$ clusters and low-spin (LS) Fe^{II} heme centers. Spectra of isolated mitochondria were largely devoid of ferritin but contained the central doublet and features arising from what appear to be Fe^{III} oxyhydroxide (phosphate) nanoparticles. Spectra from both cells and mitochondria contained a low-intensity doublet from non-heme high-spin (NHHS) Fe^{II} species. A portion of these species may constitute the 'labile iron pool' (LIP) proposed in cellular Fe trafficking. Such species might engage in Fenton chemistry to generate reactive oxygen species. EPR spectra of cells and mitochondria exhibited signals from reduced Fe/S clusters, and HS Fe^{III} heme and non-heme species. The basal redox state of mitochondria within cells is reduced as monitored by heme redox states; this redox poise is unaltered during the anaerobic isolation of the organelle. Contributions from heme *a, b* and *c* centers were quantified using electronic absorption spectroscopy. Metal concentrations in cells and mitochondria were measured using ICP-MS. Results were collectively assessed to estimate the concentrations of various Fe-containing species in mitochondria and whole cells – the first "ironome" profile of a human cell.

Iron is an essential component of human cellular metabolism, due to its extensive redox, catalytic and substrate-binding abilities (1). A comprehensive molecular-level understanding of cellular iron metabolism will not only require understanding the properties of individual Fe-containing proteins, but a systems-level understanding of iron trafficking and regulation. Connecting these two levels, a major objective of our research program, is especially challenging.

Iron is imported into the cell via two major pathways. One involves transferrin, a protein that reversibly binds Fe^{III} ions (2). The other transferrin-independent pathway involves a cell-surface ferrireductase that reduces Fe^{III} to Fe^{II} prior to uptake (3, 4). In both pathways,

*To whom correspondence should be addressed. Phone: 979-845-0956. Fax: 979-845-4719. lindahl@chem.tamu.edu. .

Supporting Information Available. A summary of whole cell batches (Table S1) and mitochondrial batches (Table S2) prepared and analyzed, packing efficiency results of whole cells and mitochondria (Table S3), transition metal concentrations from ICP-MS of whole cells and mitochondria (Table S4), additional Mössbauer spectra (Figure S1) and EM images of isolated mitochondria (Figure S2). This material is available free of charge via the Internet at http://pubs.acs.org.

Fe^{II} ions are eventually pumped into the cytosol where some incorporate into apo-proteins and others are trafficked into various cellular compartments.

Mitochondria are “traffic hubs”, as they reportedly account for 20-30% of cellular Fe (5). Cytosolic Fe enters mitochondria via mitoferrins (6) and perhaps by other unidentified transporters. Mitochondria may also import Fe by direct contact with transferrin-containing endosomes (7) and *via* the siderophore 2,5-dihydroxybenzoic acid (8). Most cellular Fe/S clusters and all heme prosthetic groups are biosynthesized in mitochondria. The final step of heme biosynthesis, inserting Fe^{II} into protoporphyrin IX, occurs in the mitochondria (9).

The Fe used to build Fe/S clusters in the mitochondria is transferred onto Fe/S scaffold proteins in the matrix of the organelle (10). These clusters are inserted into various recipient apo-proteins including respiratory complexes I – IV (11). RCI contains 2 [Fe_2S_2] clusters and 6 [Fe_4S_4] clusters (12). RCII, a.k.a. succinate dehydrogenase, contains a low-spin (LS) heme *b* as well as [Fe_2S_2], [Fe_4S_4] and [Fe_3S_4] clusters (13). RCIII, a.k.a. cytochrome bc_1, contains a [Fe_2S_2] Rieske cluster, one heme *c* and two heme *b* centers (14). Cytochrome *c* contains a LS heme *c* center, while RCIV, a.k.a. cytochrome *c* oxidase, harbors a di-copper center (Cu_A), a heme *a* center, and an active-site heme a_3 center interfaced to the Cu_B center (15).

Ferritin is a cytosolic protein complex that stores Fe as an insoluble magnetically-interacting ferrihydrite. This prevents Fe from participating in Fenton chemistry ($Fe^{II} + H_2O_2 \rightarrow Fe^{III} OH^- + \cdot OH$) (16). Ferritin can store up to ~4500 iron atoms in its inner core, estimated to correspond to 60% to 88% of total cellular iron (17). The complex also mobilizes Fe under iron-depleted conditions.

Mössbauer spectra of ferritin at low temperatures (4.2 K) exhibit a broad sextet pattern similar to mononuclear high-spin (HS) Fe^{III} complexes. At ~ 70 K and higher, the sextet collapses into a broad quadrupole doublet with Mössbauer parameters of a superparamagnetic Fe^{III} species (18). Unlike mononuclear HS Fe^{III} species, ferritin is EPR-silent at low temperatures and gives rise to a broad EPR signal in the g ~ 2 region as temperatures are raised above ~ 50 K (19).

A proportion of cellular iron has been hypothesized to be loosely coordinated and to function either as feedstock for the assembly of Fe centers or as trafficking species that can be imported into organelles. These forms of Fe are collectively referred to as the *Labile Iron Pool* (LIP). There is substantial, albeit circumstantial, evidence for an LIP in the cytosol and mitochondrial matrix (20). The mitochondrial LIP may be used for Fe-S cluster and heme biosynthesis, whereas the cytosolic LIP may report on the overall Fe status of the cell, be imported into various organelles as needed (21), and serve as feedstock for cytosolic Fe/S cluster assembly (22). Due to its weak coordination, the LIP may also participate in Fenton chemistry and thus generate ROS. ROS-promoted damage may be associated with aging and neurodegenerative diseases (21).

In this study, we evaluated, on the systems-level, the speciation and distribution of iron (i.e. the *ironome*) in whole human Jurkat cells and their mitochondria using a biophysical approach centered on Mössbauer spectroscopy but also involving EPR, UV-vis and ICP-MS. We were unable to resolve individual Fe-containing species, but could resolve different types or categories of Fe-associated species. Our results indicate that ferritin and mitochondrial Fe are indeed dominant players in cellular Fe metabolism. NHHS Fe^{II} species were detected at concentrations exceeding previous estimates, and we provide evidence for Fe^{III} oxyhydroxo nanoparticles in both isolated mitochondria and whole cells. These results were integrated into a semi-quantitative model describing the distribution and speciation of iron in a human cell.

Experimental Procedures

Bioreactor and Cell Culture

T-REx Jurkat cells (Invitrogen, R72207) were grown in a custom-built 25 L bioreactor under an atmosphere of 75% N_2, 20% O_2, and 5% CO_2 as established with a high-precision gas mixer (MG Industries). All gases were 99.9% pure (certified grade) and were delivered to the culture medium at a combined flow rate of ~ 3 mL/min. Temperature was maintained at 37° C by circulating water through the jacket of an all-glass bioreactor (Chemglass). The 12″ diameter stainless-steel lid plate had 4 evenly spaced 1″ ID ports with screw tops surrounding a central stir-motor connection. Two 1″ × 3″ and two 1″ × 30″ Teflon rods were inserted into the ports. The long rods were used to add media, harvest cells, and bubble gases through the culture. The short rods were used to deliver gases to the headspace and exhaust gases. A small hole was drilled into the short Teflon rod used to exhaust gases, through which a thin tube connected to a syringe was threaded. This tube was used to remove small samples of culture for cell count and to assess viability. A rounded-rectangular (3″ × 24″) Teflon paddlewheel was attached to the underside of the lid, and a stir-motor (Arrow Engineering Co., Inc model 350) rotated it at ~ 60 rpm. The bioreactor was wrapped with a black cloth during cell growth.

Starter cell cultures were grown in a CO_2 incubator (Nuaire, Model NU-5500), starting from a 100 mL culture, which was scaled up to 1 L once growth was evident. When the 1 L culture reached a density of ~3×10^6 cells/mL (the maximum density), it was used to inoculate 2 L of medium in the bioreactor. Additional medium was added when cells reached maximum density. When the culture volume was < 10 L, gases were delivered to the headspace *above* the liquid; when the volume was > 10 L, gases were bubbled *through* the liquid. Cells in all culture volumes were grown in RPMI 1640 medium (Sigma Aldrich) supplemented with 5% Newborn Calf Serum (Invitrogen) and an antimycotic-antibiotic cocktail (Invitrogen) to give final concentrations of 100 units/L penicillin, 100 μg/L streptomycin, 0.25 μg/L amphotericin B, and 10 μM ^{56}Fe or $^{57}Fe^{III}$ citrate. Pluronic F-68 (Sigma Aldrich) was added to a final concentration of 0.05% w/v to prevent hydrodynamic damage to the cells. Samples were removed daily and inspected by phase-contrast microscopy for viability and contamination, using 0.4% Trypan Blue solution. Cells were harvested when the cells reached maximum density. Cells were removed from the bioreactor using a peristaltic pump and centrifuged at 800×g for 10 min (Beckman Coulter Avanti J-26 XP centrifuge, JLA 8.1 rotor).

Whole cell Mössbauer and EPR sample preparation

EPR and Mössbauer samples of cells were prepared from 1 to 3 L of cultures that had reached maximum density. Cells were washed with phosphate-buffered saline (PBS, pH 7.4) containing 1 mM EGTA, followed by another wash with EGTA-free PBS buffer. Cells were then packed into 3 mL Mössbauer cups or 4 mm OD quartz EPR tubes by centrifugation at 800×g for 1 hr. The supernatant was removed and samples were frozen in liquid N_2 aerobically.

Mitochondria Isolation

Pellets of freshly harvested cells (wet weight 50-60 g) from 24 L of culture were washed twice with PBS buffer (pH 7.4). Pelleted cells were re-suspended in ~ 500 mL of degassed Mitochondria Isolation Buffer (MIB: 225 mM D-mannitol, 75 mM sucrose, 5 mM HEPES, 1 mM EGTA and 1 mM PMSF, pH 7.4) to a cell density of ~2×10^7 cells/mL. From this point onwards, all manipulations were conducted anaerobically, mostly in an Ar-atmosphere MBraun Labmaster glove box containing less than 5 ppm O_2 as monitored by a Teledyne O_2 analyzer (Model 310). For centrifugation steps, samples were sealed in airtight centrifuge

bottles inside the glove box before removing for centrifugation; afterwards, they were returned to the box before being opened for further manipulations. Cells were disrupted anaerobically by nitrogen cavitation at 800 psi for 30-40 min, using a disruption vessel (Model 4635, Parr Instruments). The cavitation extract was centrifuged at 800-times;g for 10 min and the pellet was discarded. The supernatant was centrifuged again at 9000×g for 30 min using a Sorvall Evolution centrifuge with SLA-1500 rotor. The resulting pellet, which contained crude mitochondria, was re-suspended in ~ 2 mL of MIB buffer, layered over a discontinuous gradient of 7.5 mL of 6% Percoll/3 mL of 17% Histodenz/3 mL of 35% Histodenz in MIB as described (23) and centrifuged at 45,000×g for 1 hr using a Beckman Coulter Optima L-90K ultracentrifuge with a SW 32 Ti swinging-bucket rotor. Mitochondria were collected from the 17-35% Histodenz interface and washed once with MIB. Mitochondria were then packed into Mössbauer cups by centrifugation in the ultracentrifuge (SW 32 Ti rotor) at 10,000×g for 1 hr. The supernatant was removed and the mitochondrial samples were frozen and stored in liquid N_2.

Protein concentrations

Protein concentrations were determined using a BCA Protein Assay kit (Thermo Scientific Pierce Protein Research Products) as per manufacturer‘s instructions. Bovine serum albumin (BSA) was used to generate a standard curve (0-2 mg/mL). Absorbances were measured at 562 nm.

Biophysical Studies

EPR spectra of whole cells and isolated mitochondria were collected on an X-band EMX spectrometer (Bruker Biospin Corp., Billerica, MA) equipped with an Oxford Instruments ER900A cryostat. Spin quantifications were performed with SpinCount (http://www.chem.cmu.edu/groups/hendrich/facilities/index.html), using 1.00 mM $CuSO_4$-EDTA as standard. Mössbauer spectra were acquired using a Model MS4 WRC spectrometer (SEE Co. Edina, MN) and a model LHe6T spectrometer (SEE Co., Edina MN). The latter instrument was equipped with a variable field superconducting magnet capable of generating 0 - 6 Tesla fields. Both instruments were calibrated using a spectrum of α-Fe foil collected at room temperature.

Packing Efficiencies

Jurkat cells were packed into an EPR tube by centrifugation at 800×g for 1 hr (Beckman Avanti-J26 XP centrifuge). Isolated mitochondria were similarly packed at 10000×g (Beckman Ultracentrifuge). The supernatant was discarded. Packed pellets of volume V_{pellet} consisted of the sample and interstitial buffer ($V_{\text{pellet}} = V_{\text{sample}} + V_{\text{int}}$). To determine packing efficiency, defined as $100 \cdot V_{\text{sample}}/V_{\text{pellet}}$, the pellet was re-suspended in a known volume of buffer (V_{buffer1}) containing 100 μM of a membrane-impermeable fluorescent Compound 5 (24). The sample was packed again for 1 hr. The supernatant, of volume V_{sup1} and containing Compound 5 at concentration C_{sup1}, was removed. C_{sup1} was determined using a fluorescence spectrometer (Koala 90080, ISS Inc). The conservation of matter requires that

$$V_{buffer1} \cdot (100\mu M) = \left(V_{\text{sup1}} + V_{\text{int1}}\right) \cdot C_{\text{sup1}}$$

where V_{int1} is the volume of the interstitial buffer in the pellet. This equation was solved for V_{int1} allowing the first packing efficiency ($100 \cdot V_{\text{sample1}}/V_{\text{pellet1}}$) to be determined.

The pellet was re-suspended in a known volume of buffer ($V_{buffer2}$) lacking the fluorescent compound and the suspension was packed again. In this case, the conservation of matter requires that

$$V_{int2} \cdot C_{sup1} = \left(V_{sup2} + V_{int2}\right) \cdot C_{sup2}$$

C_{sup2}, V_{sup2} and $V_{pellet2}$ were measured as above, allowing V_{int2} and a second packing efficiency ($100 \cdot V_{sample2} / V_{pellet2}$) to be calculated. The two packing efficiencies were averaged.

ICP–MS

Packed whole cells and isolated mitochondria from EPR tubes were diluted with a known volume of buffer (PBS buffer for whole cells, MIB for mitochondria). Suspensions were placed in 15 mL BD Falcon tubes and digested in concentrated trace-metal-grade nitric acid (final concentration 20-30%) for ~12 hrs. Samples were diluted with distilled and deionized water to a final acid concentration of 3%. The metal concentrations of digested samples were determined in both H_2 reaction and He collision modes using ICP-MS (Agilent Technologies model 7700x). Values obtained from both modes were adjusted for dilution factors and packing efficiencies, and then averaged.

Electron Absorption Spectroscopy

Packed cell and mitochondrial samples from EPR tubes were diluted 3-fold with isolation buffer. Suspensions were placed in a custom 2 mm pathlength quartz UV-Vis cuvette (Precision cells), sealed with a septum, and removed from the glove box. Spectra were acquired on an Hitachi U3310 spectrometer with a Head-on photomultiplier tube, then simulated using OriginPro as described (25).

Western Blots

Forty μg of protein from cell extracts or mitochondria was loaded and separated on a 12% polyacrylamide gel (Bio-Rad) using SDS-containing running buffer and 100 V potential. Proteins were transferred to Immun-Blot PVDF membranes (Bio-Rad) overnight at 20 V. The membranes were incubated for 2 hrs using Blocker™ Casein solution (Thermo Scientific). Mouse monoclonal primary antibodies (Abcam) specific to human mitochondrial porin, human endoplasmic reticular protein PDI, human nuclear protein p84 were all diluted 1:1000 and mouse monoclonal antibody specific to human lysosomal protein LAMP1 was diluted 1:10,000 in Blocker™ casein solution. Membranes were incubated with primary antibody solutions for 1 hr, followed by another blocking step for 30 min using Blocker™ casein. Membranes were then incubated with goat anti-mouse HRP conjugated secondary antibody (Invitrogen) diluted 1:3000 in Blocker™ casein solution, followed by detection using the Thermo Scientific Enhanced Chemiluminescent Western Blotting Substrate. Images were obtained using the FujiFilm LAS-4000 mini imager and analyzed using ImageJ.

Electron Microscopy

Mitochondria were fixed in 3% (v/v) glutaraldehyde in MIB, washed 3 times with MIB, fixed in 1% (v/v) osmium tetroxide, infiltrated and embedded in epoxy resin by polymerization at 60° C overnight. Ultrathin sections were obtained using an Ultracut E microtome (Reichert-Jung) and post-stained on drops of 2% (w/v) uranyl acetate and 100 mM lead citrate as described (26). EM images were obtained on a JEOL 1200 EX Transmission Electron Microscope.

Results

Analytical Characterization

Fourteen batches of Jurkat cells were grown in medium containing ~ 6 WM endogenous ^{56}Fe (as measured by ICP-MS) and supplemented with 10 μM $^{57}Fe^{III}$ citrate. The percent enrichment (*ca.* 75%) indicated that cells incorporated both sources of Fe. Mitochondria were isolated from 9 of these batches. Due to limited amounts of material, not every batch was characterized by every technique; characterizations performed on each batch are summarized in Tables S1 and S2.

Purities of 6 batches of isolated mitochondria were evaluated by Western blots. Membrane integrity from 3 batches was assessed by EM (Table S2). Western analysis indicated a 10-fold increase in the mitochondrial porin protein in isolated mitochondria relative to the same mass of cell extract protein. Isolated mitochondria contained small levels of contaminating proteins, including marker proteins LAMP1 from lysosomes, p84 from nuclei, and PDI from ER (Fig. 1, top panel). EM images of isolated mitochondria (Fig. 1) generally showed intact organelles with sharp cristae, though some unidentified density was evident. In summary, EM and Western blot analyses suggest that the isolated mitochondria used in this study were 70% - 80% pure and generally intact.

We determined the absolute concentration of metal ions and protein in 5 batches each of mitochondria and whole cells (Table 1; individual determinations in Table S4). These values were obtained by dividing observed concentrations in packed mitochondria and cells by measured packing efficiencies (65% ± 10% and 81% ± 6%) respectively. See Table S3 for individual packing efficiency results.

Biophysical characterization of mitochondria

Three batches of isolated mitochondria were analyzed by Mössbauer spectroscopy (Table S2). Results are summarized in Table 1. Low-temperature low-field Mössbauer spectra exhibited 4 distinguishable species. The spectrum from batch M04 is shown in Fig. 2A while others are given in Fig. S1. The dominating features consisted of two overlapping quadrupole doublets in the center of the spectrum. These included the central doublet (CD) with parameters typical of S = 0 $[Fe_4S_4]^{2+}$ clusters and LS ferrous heme centers (δ = 0.46 mm/s; ΔE_Q = 1.2 mm/s), and a broad doublet with parameters (δ = 0.48 mm/s and ΔE_Q = 0.57 mm/s) typical of Fe^{III} (phosphate) oxyhydroxide nanoparticles. Such particles have been observed in certain genetic strains of yeast mitochondria (27, 28). The blue and purple lines in Fig. 2A simulate these two doublets.

The magnetic properties associated with the two doublets were investigated at high applied magnetic field (Fig. 2C). The solid blue line simulates the CD and confirms that it arises from diamagnetic $[Fe_4S_4]^{2+}$ clusters and LS ferrous heme centers. The nanoparticle doublet broadened significantly at 6 T. The spectrum was compared to that of a yeast sample that was dominated by Fe^{III} oxyhydroxide nanoparticles (24). Spectral features (Fig. 2D) were similar, suggesting that the second dominant doublet in the low-field spectrum of human mitochondria arose from a similar type of nanoparticle.

Low-temperature, low-field Mössbauer spectra of human mitochondria included 3 minor features. A quadrupole doublet was simulated (brown line, Fig. 2A) with parameters typical of HS Fe^{II} hemes (δ = 1.00 mm/s; ΔE_Q = 2.00 mm/s). Another doublet was simulated using parameters (δ = 1.30 mm/s; ΔE_Q = 3.00 mm/s) typical of *non–heme* HS Fe^{II} ions coordinated by O and N donors. The concentrations of heme centers in mitochondria were quantified by electronic absorption spectroscopy (Fig. 5A and Table 1).

The 5 K 0.05 T spectrum of mitochondria also included broad features that were barely distinguishable from the baseline and were spread over the velocity range (Fig. 2A). At 70 K, these features collapsed into the center (Fig. 2B) as is typical of ferritin. At 6 T, the same features sharpened, revealing the same positions as the ferritin sextet in whole cell spectra (Fig. 2C). These features in mitochondria could arise from either contaminating ferritin, mitochondrial ferritin, or other ferritin-like material.

Low-temperature EPR of isolated mitochondria in the g = 2 region (Fig. 4A, *ii*) revealed a number of features (Fig. 4A). Spectra were decomposed into four signals with g –values indicated in Fig. 4A, *iii* – *vi*. Spin quantifications of most of these signals are given in Table 1. The signal with g = 1.98 (Fig. 4A, *vi*) may arise from Fe/S clusters but this is uncertain. The g = 2.00 signal originates from an organic radical, while the g = 1.94 signal probably arises from the $[Fe_2S_2]^+$ cluster of succinate dehydrogenase (29). A very low-intensity signal at g = 2.15 was reproducibly present (Fig. 4A, *i* and *ii*), but its origin is unknown.

The low-field region (Fig. 4B) exhibited a g = 4.3 signal assigned to non-heme HS Fe^{III} species with rhombic symmetry, as well as a signal at g = 6.0 which probably arises from the active site of cytochrome *c* oxidase in a mixed redox state, with heme a_3 and Cu_B^{III} in the Fe and Cu^I states (30). At high temperatures, a broad EPR signal in the g = 2 region developed, with inverse Curie law dependence (Fig. 4C) as is characteristic of superparamagnetic Fe^{III} oxyhydroxide nanoparticles.

Biophysical characterization of Jurkat cells

The dominant feature in the 5 K 0.05 T Mössbauer spectrum (Fig. 3A) of whole Jurkat cells was a broad sextet. This feature was simulated (brown line) with effective $\delta = 0.55$ mm/s, $\Delta E_Q = 0.25$ mm/s, and $H_{eff} = 480$ kG. This species was reminiscent of HS Fe^{III} ions in ferritin (31). At 4.3 K and 6 T (Fig. 3C), magnetic hyperfine interactions were similar to those of ferritin ($\delta = 0.54$ mm/s; $\Delta E_Q = 0.20$ mm/s; $H_{eff} = 450$ kG; $\eta = 1.00$). At 70 K, the sextet collapsed into a doublet (Fig. 3B) ($\delta = 0.50$ mm/s; $\Delta E_Q = 0.75$ mm/s), again typical of ferritin. We conclude that the sextet arises from ferritin.

Other features of the 5 K, 0.05 T Jurkat cell Mössbauer spectrum were essentially identical to those in spectra of mitochondria, including a CD, a nanoparticle doublet, a quadrupole doublet from HS Fe^{II} hemes and a doublet arising from NHHS Fe^{II} species. Low-temperature EPR spectra of cells (Fig. 4, *i* in A and B) were similar to those of isolated mitochondria, including many features in the high field region and the g = 6.0 and 4.3 signals at low field. The signals were 5-7 fold less intense in cell spectra than in mitochondrial spectra. Concentrations of Fe^{II} heme centers in cells were quantified using electronic absorption spectroscopy (Fig. 5C and Table 1).

Discussion

We determined the absolute concentrations of iron and other transition metals in Jurkat cells and mitochondria isolated from these cells by determining packing efficiencies, and then using these values to correct measured concentration of metals in packed samples. There are few previous reports of absolute metal ion concentrations in mammalian cells as most are given as Fe:protein concentration ratios. Some reports are consistent with ours (32-34) while others range from being 10-fold higher (35) to nearly 50-fold lower (36). Assuming a cellular volume of 200 fL (37) we calculate from published data (35) ~ 5 mM Fe in lymphocytes, 12 times higher than we measured. Another determination in the same type of cells indicated 0.3-0.4 μmol Fe/g protein (36), 45-fold lower than we measured. Rat intestinal epithelial cells reportedly contained ~ 1.4 μmol Fe/g protein (5), ~10-fold lower than our measurements. Besides being outside the range of concentrations that we observed,

these reported concentrations are inconsistent with the Mössbauer and EPR intensities observed here. For example, a 5 mM Fe sample would exhibit far greater % effect and spin intensities than what we observed; spectra would be unobtainable with samples that contained < 100 μM Fe. The spectroscopic intensities observed here require Fe concentrations in Jurkat cells and mitochondria within the uncertainties of the concentrations reported here.

Our results allow us to estimate the fraction of Jurkat cell volume due to mitochondria (V_{mito}/V_{cell}). Heme *a* is exclusively found in cytochrome *c* oxidase, a mitochondrial protein complex. The UV-Vis spectral absorption due to reduced heme *a* can be readily quantified. Comparing the intensity of this feature in cell vs. mitochondrial suspensions (Table 1) suggests that the fraction of cell volume due to mitochondria (V_{mito}/V_{cell}) is ≈ 0.27. Heme *c* may also be found exclusively in mitochondria (as cytochrome *c* and cytochrome bc_1), and a similar analysis suggests the same ratio. After correcting for dilution, packing efficiencies, and an estimated 25% heme-free impurities, our results indicate $V_{mito}/V_{cell} \approx 0.20 \pm 0.04$. This agrees with previous electron microscopy studies which have measured this ratio in liver cells to be 0.18 (38).

The conservation of matter suggests that

$$[Fe]_{cell} - [Fe]_{ferritin} = [Fe]_{mito} \cdot \frac{V_{mito}}{V_{cell}} + [Fe]_{other} \cdot \left(1 - \frac{V_{mito}}{V_{cell}}\right)$$

where $[Fe]_{other}$ is the average [Fe] in all non-mitochondrial compartments of the cell excluding the ferritin contribution in the cytosol. By assuming $V_{mito}/V_{cell} = 0.2$ and values in Table 1 and Fig. 6, this relationship implies that $[Fe]_{other} \sim 70$ μM. This concentration includes contributions from Fe in other organelles and cytosolic Fe other than ferritin.

Our results also allow us to estimate the concentrations of respiratory complexes in human mitochondria (Table 1). The concentration of cytochrome *c* oxidase is ~ 18 μM, half of the concentration of heme $\{a+a_3\}$. This concentration (and others in Table 1 and below) refer to moles per mitochondrial volume; the concentration within the particular subcompartment of the mitochondria where RCIV is located (the IM) will be substantially higher. Heme *a* is LS and likely contributes to the CD, while heme a_3 is HS and contributes to the HS Fe^{II} doublet.

Cytochrome *c* oxidase binds 3 Cu ions (15), suggesting that about *half* of mitochondrial Cu is associated with this enzyme. Most of the remainder may be associated with a Cu pool (39). Since no Cu^{II} EPR signals were apparent in mitochondrial spectra, most or all of the Cu ions in this pool would appear to be in the Cu^{I} state. Similar conservation-of-matter relationships suggest that the average concentrations of Cu, Mn, and Zn in non-mitochondrial locations within the cell are 6, 4, and 375 μM, respectively. Approximately 80%, 40% and 10% of the Cu, Mn, and Zn in the cell, respectively, are located in mitochondria.

About 3% of cytochrome *c* oxidase molecules are in the {Fe^{III} heme a_3 Cu_B^{I}} state and exhibit the signal at g = 6.0. This signal was considered a “transient” catalytic intermediate arising from the one-electron reduction of the oxidized O_H state (40, 41). However, our results demonstrate that it is stable and present reproducibly under non-turnover conditions in both cells and anaerobically isolated mitochondria. Establishing whether it functions in catalysis will require further study, but its presence indicates that the thermodynamic reduction potential of the heme a_3 (Fe^{III}/Fe^{II}) couple is *less positive* than that of the Cu_B^{II}/Cu_B^{I} couple under *in vivo* conditions. This conclusion is supported by a previous

determination of $E^{0'}$ = 210 mV vs. SHE for heme a_3 and 340 mV for Cu_B (42). We calculate a potential of *ca.* 170 mV for the solution in equilibrium with this site, under the (anaerobic) conditions of our experiments.

We estimate a concentration of ~ 4 μM for RCIII (cytochrome bc_1) in mitochondria, based primarily on the spin concentration of the g = 1.90 signal which we assign to the Rieske Fe/S cluster. RCIII contains 1 and 2 equiv/mol of LS heme c_1 and LS heme *b*, respectively (14), both of which would have contributed to the CD in our study.

We estimate a similar concentration for RCII, based on the spin concentration of the g = 1.94 signal which presumably arises from the RCII $[Fe_2S_2]^{1+}$ cluster (25, 29). This enzyme also contains 1 LS Heme *b*, an $[Fe_3S_4]$ cluster and an $[Fe_4S_4]$ cluster (13). Collectively, the heme *b* contribution of both respiratory complexes is ~ 8 μM, suggesting that ~ 14 μM of heme *b* is due to other mitochondrial proteins such as catalase and cytochrome *c* peroxidase. The heme *c* contribution from cytochrome bc_1 is minor, suggesting that the concentration of cytochrome *c* in mitochondria is ~ 70 μM.

Heme *c* centers are LS, as is heme *a* of cytochrome *c* oxidase and, we estimate, about half of the heme *b* centers. Collectively, this corresponds to ~ 100 μM or *ca.* 9% of mitochondrial Fe. This Fe would contribute to the CD. Since the CD represents ~ 27% of the Fe in the mitochondria, we conclude that ~ 17% (200 μM) is due to Fe in the form of $[Fe_4S_4]^{2+}$ clusters. After subtracting ~ 4 μM $[Fe_4S_4]$ for the cluster in RCII, ~ 46 μM remains for other $[Fe_4S_4]$-containing proteins in mitochondria.

The ratios of RCI:RCIII:RCIV have been measured in rat and bovine tissues to be *ca.* 1:3:8 (43). The ratio of RCIII:RCIV in our mitochondrial samples was 3:18, which suggests an RCI concentration between 0.5 and 1 μM. Since RCI contains 6 $[Fe_4S_4]$ clusters and 2 $[Fe_2S_2]$ clusters (12), ~ 6 μM of $[Fe_4S_4]$ clusters due to RCI would contribute to the CD, leaving ~ 40 μM $[Fe_4S_4]$ clusters for the other mitochondrial proteins. As with yeast mitochondria (25), the concentration of $[Fe_2S_2]^{2+}$ clusters in human mitochondria appears to be low since a doublet due to this species was not detected.

Our calculations indicate that *ca.* 20% of the cell volume is due to mitochondria; this implies that ~ 55% of the Fe in the cell should be mitochondrial. Of this, *ca.* 27% (60 μM) is due to the CD. This corresponds to ~ 12% of the Fe in the cell spectrum. But the CD in the cell spectrum represents 27% of spectral intensity, corresponding to ~100 μM. The difference (100 – 60 = 40 μM) represents $[Fe_4S_4]^{2+}$ clusters and/or LS Fe^{II} hemes in the cell that are not in mitochondria.

Cells contain ~ 30 μM of HS Fe^{II} species in the cytosol. A portion of these are probably associated with the LIP, as this has been suggested to be mostly in the Fe^{II} state (44). The size of the LIP has been estimated to be between 0.5 – 10 μM in mammalian cells (45, 46), and our results are consistent with this. However, our results cannot exclude the possibility that the concentration of the LIP in human cells is 3 – 60 fold higher than these previous estimates.

Fe^{III} oxyhydroxide nanoparticles are present in both mitochondria and whole cells, at concentrations of ~ 410 and 70 μM, respectively. Similar nanoparticles have been observed in mitochondria and vacuoles of yeast cells (24, 25) where they are associated with phosphate or polyphosphate groups. At high fields, the Mössbauer spectra of the nanoparticles in yeast exhibit a wide distribution of hyperfine fields (47). In contrast, the magnetically interacting Fe^{III} ions in ferritin afford a narrow distribution of fields (48, 49). The nanoparticles observed in Jurkat cells and mitochondria also exhibited a wide distribution of hyperfine fields, suggesting that they, like their yeast counterparts, have

phosphate groups associated. These particles might be independent of ferritin or found in partially loaded ferritin; we are currently working to distinguish these possibilities.

Our results also provide insight into the redox status of the mitochondria *within* Jurkat cells, at least when packed into Mössbauer/EPR tubes. In contrast, mitochondria were isolated anaerobically. Almost all heme centers (and the same group of Fe/S clusters) in both anaerobically isolated mitochondria and in whole cells (grown in air, then packed into cuvettes) were reduced. The only exception was a small portion of heme a_3 in cytochrome *c* oxidase which was partially oxidized in both types of samples.

The distribution of iron within Jurkat cells and mitochondria are summarized in Fig. 6. A surprisingly large portion of the Fe in mitochondria is present as Fe^{III} oxyhydroxide (phosphate) nanoparticles, which might be in equilibrium with the nonheme HS Fe^{II} and Fe^{III} species in the organelle. Similar species in yeast mitochondria may function as feedstock for Fe/S cluster and heme biosynthesis (24, 25). Respiratory complexes (including cytochrome *c*) account for ~17% of mitochondrial Fe. Another 14% is present as "other" $[Fe_4S_4]^{2+}$ clusters and heme *b* centers. About 15% of mitochondrial Fe is ferritin-like; this may be a contaminant of cytosolic ferritin or ferritin-like material within the mitochondria (mitochondrial ferritin?). Approximately 20% of the volume of Jurkat cells is occupied by mitochondria, yet this fraction accounts for about *55%* of the total Fe. Another 40% of cellular Fe is stored in the cytosol as ferritin and the remaining 5% is present (outside of the mitochondria) as Fe/S containing proteins, nonheme HS Fe^{II} and Fe^{III} species. Thus, the vast majority of Fe in human cells is either *stored* (as ferritin) or *used* (within mitochondria). The bulk of the latter Fe is used to synthesize Fe/S clusters and heme centers that are primarily installed in respiratory complexes, which are used, in turn, to generate cellular energy. Only ~ 5% of cellular Fe is used for all other Fe-associated processes. This does not imply a lesser functional importance for these other process; we simply lack the resolution and sensitivity required to further characterize the Fe species associated with these processes.

The ironomes of yeast and human cells are remarkably similar. From the perspective of this study, the ironome of human mitochondria appears midway between that of fermenting and respiring yeast mitochondria. The redox poise of the organelle and the relative proportion of Fe-containing species contained therein are similar. Clearly, yeast provides an excellent model of human cells for studying Fe metabolism.

We find it intriguing that human mitochondria contain oxyhydroxide (phosphate) nanoparticles similar to those found in yeast. We suspect that they are formed independent of ferritin, in which case they would probably *not* be under the genetic control of the cell. The significant levels of NHHS Fe^{II} in human cells are also potentially significant, in that this type of Fe can generate ROS through Fenton chemistry. We plan to investigate how these nanoparticle and nonheme HS Fe^{II} species change under different growth and genetic conditions. We hope to establish how the formation of these species can be controlled, which may improve our ability to understand the molecular basis of Fe-associated diseases.

Supplementary Material

Refer to Web version on PubMed Central for supplementary material.

Acknowledgments

Compound 5 was a generous gift from Kevin Burgess (Texas A&M University). We thank Ann Ellis and Rick Littleton at the Microscopy and Imaging Center at Texas A&M University for help in collecting images. This study was supported by the National Institutes of Health (GM084266) and the Robert A. Welch Foundation (A1170).

Funding Statement: The National Institutes of Health (GM084266) and the Robert A. Welch Foundation (A1170) sponsored this study.

Abbreviations

LIP	labile iron pool
ICP-MS	inductively coupled plasma mass spectrometry
ROS	reactive oxygen species
EPR	electron paramagnetic resonance
HS	high-spin
LS	low spin
CD	central doublet
NHHS	nonheme high-spin
RCI – RCIV	mitochondrial respiratory complexes I – IV

References

1. Anderson GJ, Vulpe CD. Mammalian iron transport. Cell. Mol. Life Sci. 2009; 66:3241–3261. [PubMed: 19484405]
2. Huebers H, Josephson B, Huebers E, Csiba E, Finch C. Uptake and release of iron from human transferrin. Proc. Natl. Acad. Sci. 1981; 78:2572–2576. [PubMed: 6941310]
3. Hider RC. Nature of nontransferrin-bound iron. European Journal of Clinical Investigation. 2002; 32:50–54. [PubMed: 11886432]
4. Jordan I, Kaplan J. The mammalian transferrin-independent iron transport system may involve a surface ferrireductase activity. Biochem. J. 1994; 302:875–879. [PubMed: 7945215]
5. Richmond VS, Worwood M, Jacobs A. The Iron Content of Intestinal Epithelial Cells and Its Subcellular Distribution: Studies on Normal, Iron-Overloaded and Iron-Deficient Rats. British Journal of Haematology. 1972; 23:605–614. [PubMed: 4344207]
6. Shaw GC, Cope JJ, Li L, Corson K, Hersey C, Ackermann GE, Gwynn B, Lambert AJ, Wingert RA, Traver D, Trede NS, Barut BA, Zhou Y, Minet E, Donovan A, Brownlie A, Balzan R, Weiss MJ, Peters LL, Kaplan J, Zon LI, Paw B. Mitoferrin is essential for erythroid iron assimilation. Nature Letters. 2006; 440:96–100.
7. Sheftel AD, Zhang A-S, Brown C, Shirihai OS, Ponka P. Direct interorganellar transfer of iron from endosome to mitochondrion. Blood. 2007; 110:125–132. [PubMed: 17376890]
8. Devireddy LR, Hart DO, Goetz D, Green MR. A Mammalian Siderophore Synthesized by an Enzyme with a Bacterial Homologue Involved in Enterobactin Production. Cell. 2010; 141:1006–1017. [PubMed: 20550936]
9. Ajioka RS, Phillips JD, Kushner JP. Biosynthesis of heme in mammals. Biochimica et Biophysica Acta. 2006; 1763:723–736. [PubMed: 16839620]
10. Pandolfo M, Pastore A. The pathogenesis of Friedreich ataxia and the structure and function of frataxin. J Neurol. 2009; 256:9–17. [PubMed: 19283345]
11. Ye H, Rouault TA. Human Iron-Sulfur Cluster Assembly, Cellular Iron Homeostasis, and Disease. Biochemistry. 2010; 49:4945–4956. [PubMed: 20481466]
12. Carroll J, Fearnley IM, Skehel JM, Shannon RJ, Hirst J, Walker JE. Bovine Complex I is a complex of 45 different subunits. The Journal of Biological Chemistry. 2006; 281:32724–32727. [PubMed: 16950771]
13. Cecchini G. Function and structure of Complex II of the respiratory chain. Annual Reviews. 2003; 72:77–109.
14. Crofts AR. The cytochrome *bc1* complex: function in the context of structure. Annu. Rev. Physiol. 2004; 66:689–733. [PubMed: 14977419]

15. Tsukihara T,H,A, Yamashita E, Tomizaki T, Yamaguchi H, Shinzawa-Itoh K, Nakashima R, Yaono R, Yoshikawa S. The whole structure of the 13-subunit oxidized cytochrome c oxidase at 2.8 A. Science. 1996; 272:1136–1144. [PubMed: 8638158]
16. Theil EC. Ferritin: Structure, Gene Regulation, and Cellular Function in Animals, Plants and Microorganisms. Ann. Rev. Biochem. 1987; 56:289–315. [PubMed: 3304136]
17. Dubiel SM, Zablotna-Rypien B, Mackey JB, Williams JM. Magnetic properties of human liver and brain ferritin. Eur Biophys J. 1999; 28:263–267. [PubMed: 10192938]
18. Papaefthymiou GC. The Mössbauer and magnetic properties of ferritin cores. Biochimica et Biophysica Acta. 2010; 1800:886–897. [PubMed: 20363296]
19. Baader SL, Bill E, Trautwein AX, Bruchelt G, Matzanke BF. Mobilization of iron from cellular ferritin by ascorbic acid in neuroblastoma SK-N-SH cells: an EPR study. FEBS Letters. 1996; 381:131–134. [PubMed: 8641421]
20. Glickstein H, El RB, Shvartsman M, Cabantchik ZI. Intracellular labile iron pools as direct targets of iron chelators: a fluorescence study of chelator action in living cells. Blood. 2005; 106:3242–3250. [PubMed: 16020512]
21. Kruszewski M. Labile iron pool: the main determinant of cellular response to oxidative stress. Mutation Research. 2003; 531:81–92. [PubMed: 14637247]
22. Lill R, Mühlenhoff U. Iron-sulfur-protein biogenesis in eukaryotes. TRENDS in Biochemical Sciences. 2005; 30:133–141. [PubMed: 15752985]
23. Wiley SE, Rardin MJ, Dixon JE. Localization and function of the 2Fe-2S outer mitochondrial membrane protein MitoNEET. Methods in Enzymology. 2009; 456:233–246. [PubMed: 19348892]
24. Cockrell AL, Holmes-Hampton GP, McCormick SP, Chakrabarti M, Lindahl PA. Mössbauer and EPR Study of Iron in Vacuoles from Fermenting Saccharomyces cerevisiae. Biochemistry. 2011; 50:10275–10283. [PubMed: 22047049]
25. Morales JG, Holmes-Hampton G, Miao R, Guo Y, Münck E, Lindahl PA. Biophysical Characterization of Iron in Mitochondria Isolated from Respiring and Fermenting Yeast. Biochemistry. 2010; 49:5436–5444. [PubMed: 20536189]
26. Ellis EA. Poststaining grids for Transmission Electron Microscopy. Methods in Molecular Biology. 369:97–106.
27. Miao R, Martinho M, Morales JG, Kim H, Ellis A, Lill R, Hendrich MP, Münck E, Lindahl PA. EPR and Mössbauer Spectroscopy of Intact Mitochondria Isolated from Yah1p-Depleted Saccharomyces cerevisiae. Biochemistry. 2008; 47:9888–9899. [PubMed: 18717590]
28. Miao R, Kim H, Koppolu MK, Ellis A, Scott RA, Lindahl PA. Biophysical Characterization of the iron in mitochondria from Atm1p-depleted *Saccharomyces cerevisiae*. Biochemistry. 2009; 48:9556–9568. [PubMed: 19761223]
29. Hudder BN, Morales JG, Stubna A, Münck E, Hendrich MP, Lindahl PA. Electron paramagnetic resonance and Mössbauer spectroscopy of intact mitochondria from respiring *Saccharomyces cerevisiae*. J Biol Inorg Chem. 2007; 12:1029–1053. [PubMed: 17665226]
30. Beinert H. EPR Spectroscopy of components of mitochondrial electron-transfer system. Methods in Enzymology. 1978; LIV:133–150. [PubMed: 215873]
31. Hunt C, Pankhurst QA, Dickson DPE. Applied field Mössbauer studies of the iron storage proteins ferritin and haemosiderin. Hyperfine Interactions. 1994; 91:821–826.
32. Tangerås A, Flatmark T, Bäckström D, Ehrenberg A. Mitochondrial iron not bound in heme and iron-sulfur centers: estimation, compartmentation and redox state. Biochimica et Biophysica Acta. 1980; 589:162–175. [PubMed: 6243966]
33. Tangerås A. Iron content and degree of lipid peroxidation in liver mitochondria isolated from iron-loaded rats. Biochimica et Biophysica Acta. 1983; 757:59–68. [PubMed: 6838907]
34. Kim Y-M, Chung H-T, Simmons RL, Billiar TR. Cellular Non-Heme Iron Content Is a Determinant of Nitric Oxide-mediated Apoptosis, Necrosis, and Caspase Inhibition. The Journal of Biological Chemistry. 2000; 275:10954–10961. [PubMed: 10753895]
35. Ekmekcioglu C, Prohaska C, Pomazal K, Steffan I, Schernthaner G, Marktl W. Concentrations of seven trace elements in different hematological matrices in patients with type 2 diabetes as

compared to healthy controls. Biological Trace Element Research. 2001; 79:205–219. [PubMed: 11354346]

36. Carpentieri U, Myers J, Thorpe L, Daeschner CW III, Haggard ME. Copper, Zinc, and Iron in Normal and Leukemic Lymphocytes from Children. Cancer Research. 1986; 46:981–984. [PubMed: 3455680]
37. Chapman EH, Kurec AS, Davey FR. Cell volumes of normal and malignant mononuclear cells. J Clin Pathol. 1981; 34:1083–1090. [PubMed: 6975780]
38. Weibel ER, Stäubli W, Gnägi HR, Hess FA. Correlated Morphometric and Biochemical Studies on the Liver Cell. The Journal of Cell Biology. 1969; 42:68–91. [PubMed: 4891915]
39. Leary SC, Winge DR, Cobine PA. "Pulling the plug" on cellular copper: The role of mitochondria in copper export. Biochimica et Biophysica Acta. 2009; 1793:146–153. [PubMed: 18522804]
40. Jancura D, Berka V, Antalik M, Bagelova J, Gennis RB, Palmer G, Fabian M. Spectral and Kinetic Equivalence of Oxidized Cytochrome c Oxidase as Isolated and "Activated" by Reoxidation. The Journal of Biological Chemistry. 2006; 281:30319–30325. [PubMed: 16905536]
41. Kaila VRI, Verkhovsky MI, Wikström M. Proton-Coupled Electron Transfer in Cytochrome Oxidase. Chem. Rev. 2010; 110:7062–7081. [PubMed: 21053971]
42. Lanne B, Väangård T. Redox Titrations of Cytochrome *c* Oxidase: An Analysis of a Multi-Electron System. Biochimica et Biophysica Acta. 1978; 501:449–457. [PubMed: 204344]
43. Lenaz G, Genova ML. Structure and organization of mitochondrial respiratory complexes: a new understanding of an old subject. Antioxidants & Redox Signaling. 2010; 12:961–1008. [PubMed: 19739941]
44. Epsztejn S, Kakhlon O, Glickstein H, Breuer W, Cabantchik ZI. Fluorescence Analysis of the Labile Iron Pool of Mammalian Cells. Analytical Biochemistry. 1997; 248:31–40. [PubMed: 9177722]
45. Petrat F, Groot HD, Rauen U. Subcellular distribution of chelatable iron: a lase scanning microscopic study in isolated hepatocytes and liver endothelial cells. Biochem. J. 2001; 356:61–69. [PubMed: 11336636]
46. Gackowski D, Kruszewski M, Banaszkiewicz Z, Jawien A, Olinski R. Lymphocyte labile iron pool, plasma iron, transferrin saturation and ferritin levels in colon cancer patients. Acta Biochimica Polonica. 2002; 49:269–272. [PubMed: 12136950]
47. Seguin A, Sutak R, Bulteau A-L, Garcia-Serres R, Oddou J-L, Lefevre S, Santos R, Dancis A, Camadro J-M, Latour J-M, Lesuisse E. Evidence that yeast frataxin is not an iron storage protein in vivo. Biochimica et Biophysica Acta. 2010; 1802:531–538. [PubMed: 20307653]
48. Bauminger ER, Cohen SG, Dickson DPE, Levy A, Ofer S, Yariv J. Mössbauer spectroscopy of *Escherichia coli* and its iron-storage protein. Biochimica et Biophysica Acta. 1979; 623:237–242. [PubMed: 6994819]
49. St. Pierre TG, Bell SH, Dickson DPE, Mann S, Webb J, Moore GR, Williams RJP. Mössbauer spectroscopic studies of the cores of human, limpet and bacterial ferritins. Biochimica et Biophysica Acta. 1985; 870:127–134. [PubMed: 3081032]

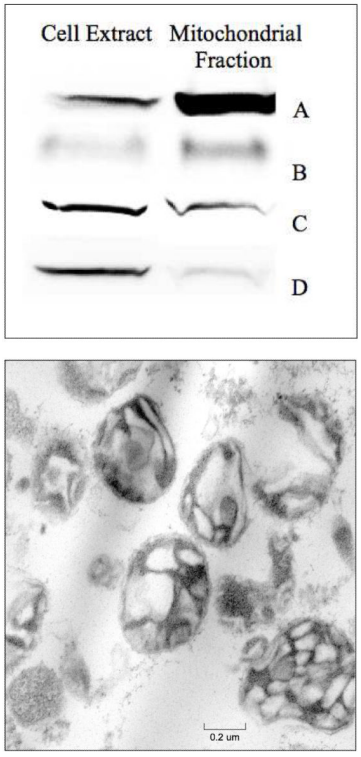

Figure 1.
Characterization of isolated mitochondria. Top, western blot of isolated mitochondria; A, Porin (mitochondria); B, LAMP1 (lysosomes); C, Endoplasmic reticulum (PDI); and D, p84 (nuclei). Bottom, electron micrograph of isolated mitochondria, magnification = 40,000×.

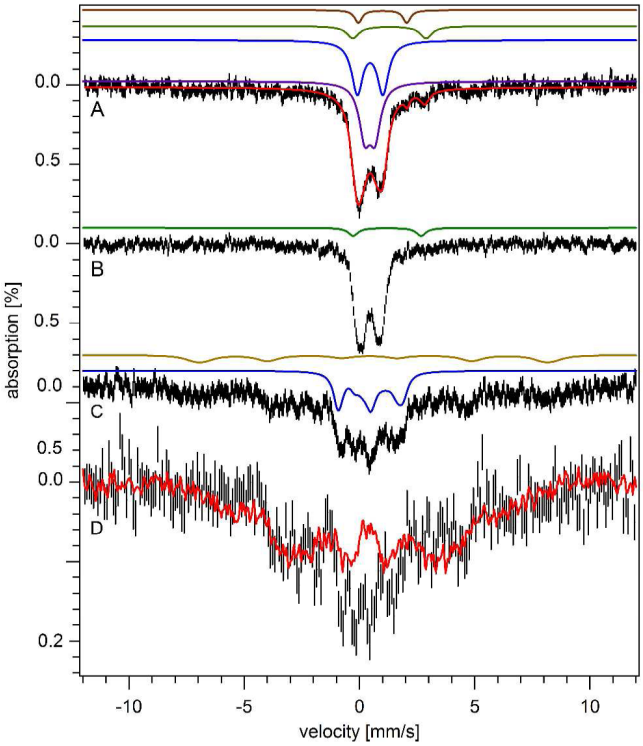

Figure 2.

Mössbauer spectra of mitochondria isolated from Jurkat cells. A, 5 K and 0.05 T; the red line is a total simulation (see Table 1 for percentages); B, same as A but at 70 K, with simulation of NHHS Fe^{II}; C, same as A except at 6 T and 4.3 K. The brown line simulates the ferritin sextet while the blue line simulates the CD; D, same as C but after subtraction of sextet and CD simulations. The red line is a 6 T, 4.3 K spectrum of yeast mitochondria isolated from Aft1-1^{up} cells (24). The applied magnetic field was parallel to the γ radiation in A and B, perpendicular in C and D.

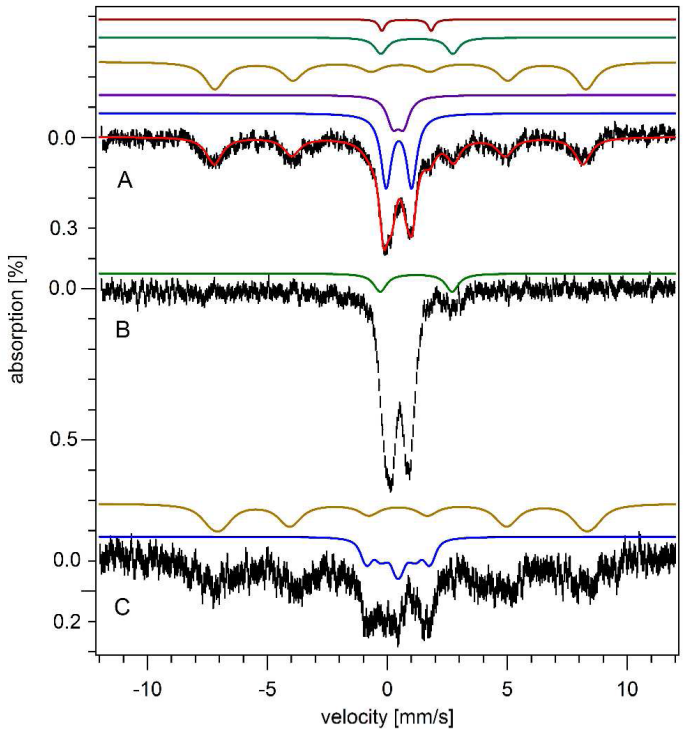

Figure 3.

Mössbauer spectroscopy of Jurkat cells. A, 5 K and 0.05 T. Colored lines above the spectrum are individual simulations; the overlaid red line is a total simulation (see Table 1 for percentages). B, 70 K 0.05 T. The green line simulates the NHHS Fe^{II} doublet. C, 6 T and 4.3 K. The brown and blue lines simulate the sextet and CD respectively.

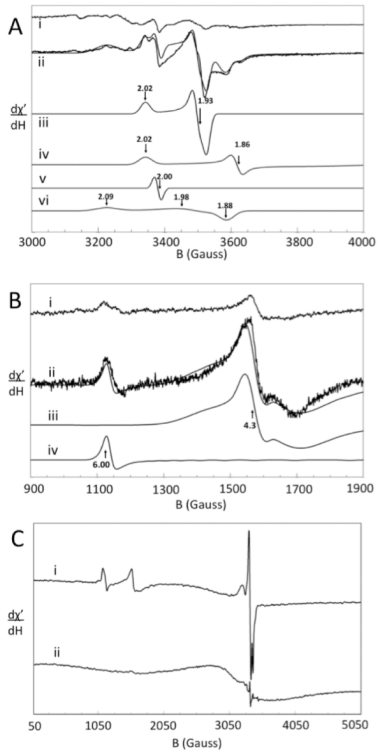

Figure 4.

X-band EPR spectra of Jurkat cells and mitochondria. A, high-field region of (*i*) cells and (*ii*) mitochondria (ave. of 5 and 3 scans, respectively). Simulations *iii, iv, v,* and *vi* were of the g_{ave} = 1.94, 1.90, 2.00, and 1.98 signals, respectively. The solid line overlaying *ii* is a combined simulation. Temperature, 8 K; frequency, 9.47 GHz; microwave power, 2.012 mW. B, low-field region of (*i*) cells and (*ii*) mitochondria (ave. of 5 and 3 scans, respectively). Simulations *iii* and *iv* are of the g = 4.3 and 6.0 features, respectively. The solid line overlaying *ii* is a combined simulation (same EPR conditions). C, wide-sweep spectra of mitochondria at 8 K (*i*) and 80 K (*ii*). Frequency, 9.46 GHz, power, 20.12 mW. In all spectra, modulation amplitude was 10 G, modulation frequency, 100 kHz, conversion time, 164 ms, and sweep time, 336 sec.

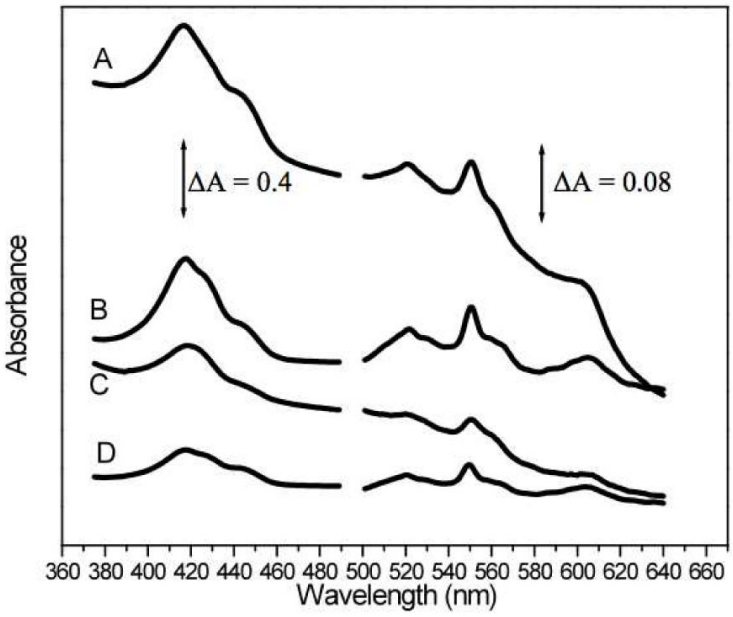

Figure 5.
Electronic absorption spectra of mitochondrial (A) and cell (C) suspensions. Simulated spectra B and D were generated by combining individual spectra of isolated proteins containing the different types of hemes.

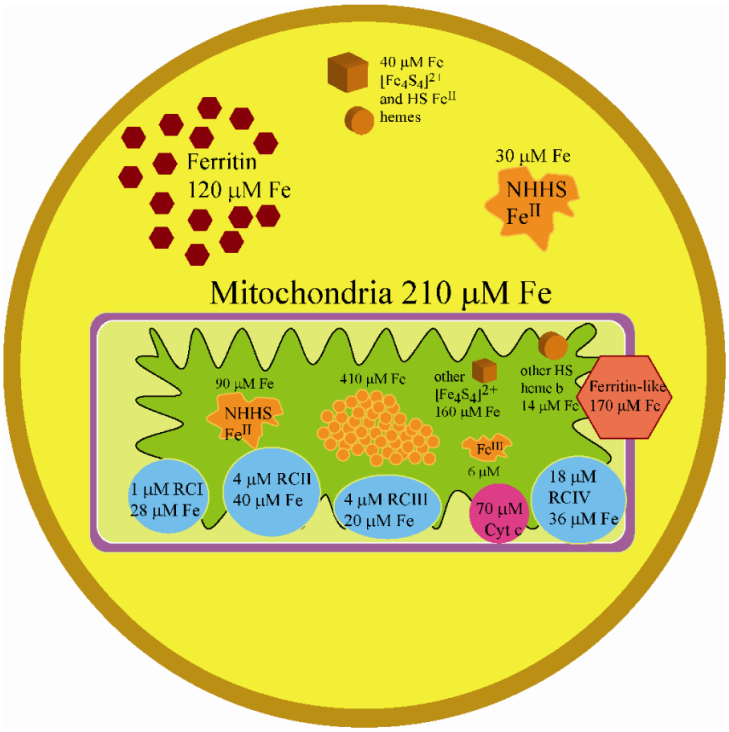

Figure 6.
Ironome profile of Jurkat cells and mitochondria. See text for details.

Table 1

Analytical properties of whole Jurkat cells and isolated mitochondria. Reported metal, UV-vis and EPR concentrations refer to packed cells and mitochondria after dividing by packing efficiencies. Values reported for isolated mitochondria were obtained by also dividing measured values by 0.75, to account for presumed metal-free impurities. The absolute uncertainty in percentages obtained by Mössbauer spectroscopy is ± 3%. Replicates n is given in the column to the right of the corresponding parameter. Concentrations of respiration-related mitochondrial proteins are estimated from the collective results of this study.

	Mitochondria	***n***	**Whole Cells**	***n***
Protein (mg/mL)	52 ± 12	4	62 ± 11	4
[Fe] (μM)	1120 ± 95	5	400 ± 70	5
[Cu] (μM)	115 ± 8	5	28 ± 4	5
[Zn] (μM)	167± 94	5	408 ± 135	5
[Mn] (μM)	14 ± 3	5	7.2 ± 0.6	5
Fe^{III} oxyhydroxy nanoparticles (%)	37	3	18	2
Ferritin-like (%)	15	3	40	2
Central Doublet (%)	27	3	27	2
Non-Heme HS Fe^{II}	8	3	11	2
HS FeII Hemes	4	3	4	2
g = 1.94 (μM)	3.3 ± 0.6	4	0.3±0.1	4
g = 1.90 (μM)	3.3 ± 0.6	4	0.3±0.1	4
g = 2.00 (μM)	0.2 ±0.06	4	~ 0	4
g = 4.3 (μM)	6 ±0.6	4	1.5 ± 0.5	4
g = 6.0 + (6.4, 5.4)	0.5 ±0.3	4	~ 0	4
Reduced [Heme *a*] (μM)	37 ± 5	4	10 ± 2	4
Reduced [Heme *b*] (μM)	21 ± 4	4	5 ± 2	4
Reduced [Heme *c*] (μM)	75 ± 11	4	20 ± 3	4
Cytochrome *c* oxidase (μM)	~ 18		n/a	
Cytochrome *c* (μM)	~ 70		n/a	
Cytochrome bc_1 (μM)	~ 4		n/a	
Succinate Dehydrogenase (μM)	~ 4		n/a	
Respiratory Complex I (μM)	~ 1		n/a	